Available online at www.sciencedirect.com
SCIENCE DIRECT®
Energy and Buildings 38 (2006) 502–514
ENERGY and BUILDINGS
www.elsevier.com/locate/enbuild

Model-based analysis and simulation of regenerative heat wheel

Zhuang Wu [a], Roderick V.N. Melnik [b,*], Finn Borup [c]

[a] Department of Control Engineering, Aalborg University, Fredrik Bajers Vej 7C, Aalborg, DK-9220, Denmark
[b] Mathematical Modelling and Computational Sciences, Wilfrid Laurier University, 75 University Avenue West, Waterloo, ON, Canada N2L 3C5
[c] OJ Electronics A/S, Stenager 13B, Sønderborg DK6400, Denmark

Received 26 April 2005; received in revised form 18 August 2005; accepted 22 August 2005

Abstract

The rotary regenerator (also called the heat wheel) is an important component of energy intensive sectors, which is used in many heat recovery systems. In this paper, a model-based analysis of a rotary regenerator is carried out with a major emphasis given to the development and implementation of mathematical models for the thermal analysis of the fluid and wheel matrix. The effect of heat conduction in the direction of the fluid flow is taken into account and the influence of variations in rotating speed of the wheel as well as other characteristics (ambient temperature, airflow and geometric size) on dynamic responses are analysed. The numerical results are compared with experimental measurements and with theoretical predications of energy efficiencies.
© 2005 Elsevier B.V. All rights reserved.

Keywords: Heat recovery systems; Heat transfer in rotary regenerators; Numerical methods; Modeling

1. Introduction

Mechanical ventilation with heat recovery systems plays a vital role in securing optimum air quality, thermal comfort and saving thermal energy [1]. It is often considered as one of the dominant elements of low energy residential buildings in cold winter regions [2]. Estimates show that as much as 70% of the energy lost through mechanical ventilation (balanced or extract) can be recovered by the use of ventilation heat recovery systems [3]. Such systems have a significant effect on the energy effectiveness of the entire ventilation unit and control system (see Fig. 1). The rotary regenerator is a key element of the thermal model for this system, while other components (such as the frequency converter, ac motor, air fan, air filter, duct and various sensors) are intrinsic elements of the airflow model. A better understanding of the dynamics of the heat wheel is an important prerequisite to more efficient designs of the heat recovery systems and modeling constitutes a powerful tool in achieving this goal.

The importance of modeling the dynamics of the heat wheel follows from the following fact. As soon as heating is required, the wheel speed will first increase in the heat recovery unit, which leads to a possibility of control of supplied air heating even in the situations where the outdoor temperature is very low. The main parameters for the control of the ventilation unit are the temperature and airflow. Therefore, a closed-loop control system for temperature regulation and airflow regulation applied with conventional PI controllers can be formed to implement the performance of the entire regulation system, as demonstrated in Fig. 1.

The focus of our study in this paper is the model-based analysis and simulation of the heat wheel. Firstly, based on physical principles, we will develop a mathematical model of the heat wheel and implement it with the developed computational procedure. Secondly, we will analyse the temperature distribution and its variations in time and will investigate how the airflow, temperature and rotational speed of the wheel influence upon the dynamic response. Our discussion is centered around a comprehensive model for the analysis of the heat wheel with high energy efficiency which constitutes a fundamental block of the temperature control system design.

The model construction discussed in the subsequent sections rests on the following observation. In the rotary regenerator under consideration, both hot and cold fluids (gases) flow through the same flow passage alternatively and hence heat flows intermittently. The flow passage (or the heat transfer

* Corresponding author. Tel.: +1 519 884 1970; fax: +1 519 884 9738.
E-mail address: rmelnik@wlu.ca (R.V.N. Melnik).

0378-7788/$ – see front matter © 2005 Elsevier B.V. All rights reserved.
doi:10.1016/j.enbuild.2005.08.009

Nomenclature

A	heat flow cross-area (m^2)
A_w	cross-area of matrix (m^2)
B_w	width of the surface through which heat transfer (m)
c_p	specific heat at constant pressure (J/(kg °C))
C	flow stream thermal capacity rate of one side (J/(s °C))
C_r	ratio of heat capacity of the matrix to the minimum air heat capacity rate in a rotary air-to-air heat exchanger, thermal capacitance
d	diameter of flute (m)
D	inside diameter of the circular tube on one side estimated by all the free-flow flute (m)
h	convective heat transfer coefficient of fluid flow (W/(m^2 °C))
k	thermal conductivity (W/(m °C))
L	length of heat wheel (m)
$\dot{m}$	mass flow rate (kg/s)
M	mass (kg)
Nu	Nusselt number
NTU	number of transfer unit
Pr	Prandtl number
q''	heat flux, heat transfer rate per unit of surface area (J/(s m^2))
$\dot{Q}$	heat transfer rate on whole cross-area (J/s)
R	heat transfer resistance (m^2 °C/W)
Ratio	ratio of minimum to maximum air heat capacity rates in an air-to-air heat exchanger
Re	Reynold number
T	temperature (K)
U	total heat transfer coefficient (W/(m^2 °C))
v	velocity of airflow (m/s)
$\dot{v}$	volumetric airflow rate (m^3/s)

Greek letters

ε_{cf}	effectiveness of counter flow heat exchanger
ϕ	rotational frequency (revolution per second) '(Hz (s^{-1}))
μ	absolute viscosity coefficient (kg/(m s))
ν	kinematic viscosity coefficient (m^2/s)
ρ	density (kg/m^3)

Subscripts

c	cold fluid side of heat exchanger
h	hot fluid side of heat exchanger
w	wheel matrix
f	fluid
in	inlet
out	outlet
max	maximum value
min	minimum value
hy	hydraulic

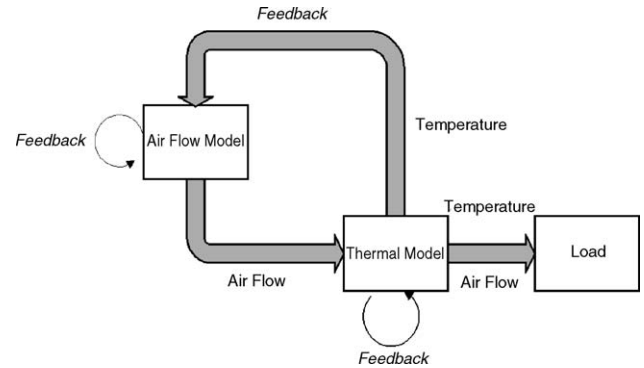

Fig. 1. Concept of the entire ventilation unit control system integrated with temperature control and airflow control.

surface) is generally made of metals with cellular structure and is referred to as a wheel matrix. The wheel rotates at very low speeds with a constant fraction of the core facing partially for the hot and cold fluids. When the hot gas flows over the heat transfer surface (through the flow passage), the thermal energy is stored in the matrix wall. When the cold gas flows through the same passage at a later stage, the matrix wall delivers the thermal energy to the cold fluid. Thus, heat is not transferred continuously through the wall as in a direct transfer type exchanger, but is alternately stored and rejected by the matrix wall [4,5].

The subsequent sections of the paper are organised as follows. In Section 2, we develop a mathematical model describing the dynamics of the heat wheel. Basic assumptions and limitations of the model are also formulated in this section as well as the procedure for evaluating the overall heat transfer coefficient. The influence of frequency on performance of the model is also discussed in this section. In Section 3, we provide the details of our computational procedure and present the developed numerical algorithm for the solution of the problem. In Section 4, we discuss validation of the model by experimental data and give details on comparisons of our numerical results with available theoretical predictions. Conclusions are given in Section 5.

2. Mathematical modeling of heat wheel

The main goal of this section is to develop a mathematical model for the heat wheel dynamics. In what follows, we start our discussion with basic physical principles, formulate necessary simplifying assumptions and derive the model based on the energy balance equation. Since accounting for temperature variations of the fluid airflow and matrix involves the determination of the total heat transfer coefficient, we discuss this issue in details. The effect of the rotating speed of the wheel on the performance of the model is also analysed. All necessary specifications and estimates of the parameters that are employed in this section are listed in 'Nomenclature' and Table A.1 given in the end of the paper.

2.1. Physical principles and simplifying assumptions

A rotary air-to-air heat wheel can be viewed as a periodic-flow type heat exchanger. The matrix (see Fig. 2) is rotated so

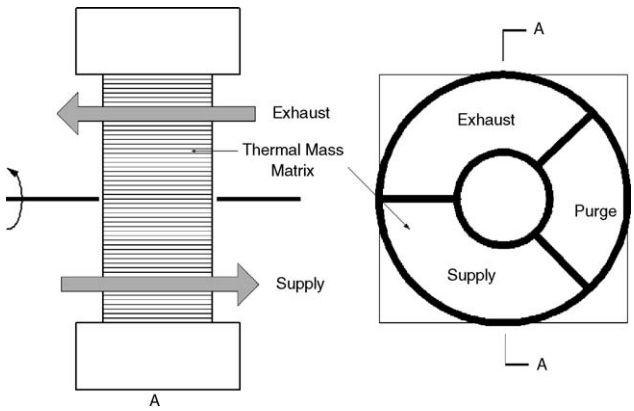

Fig. 2. Schematic diagram of the heat wheel operating principle.

that the element is periodically passed from the hot fluid through the matrix to the cold fluid. The wheel is designed to be positioned between two adjacent ducts with opposing flow directions. Therefore, it is expected that the characteristics of the heat wheel under consideration approach those of the conventional two-fluid counter flow heat exchanger.

The development of the mathematical model describing the dynamics of the heat wheel is based on the following simplifying assumptions (see also [6,7]):

- the flow is incompressible and is considered here as a one-dimensional flow;
- the thermal properties of the fluids (such as specific heat, thermal conductivity, density) are assumed to have bulk average values and be uniform at any cross-section;
- the mass flow rate is constant for each flow fluid;
- thermal conduction in both the wheel matrix and the fluids is assumed to be parallel to the flow direction, while axial conduction is assumed to be negligible;
- the convection heat transfer coefficient (denoted by h) is assumed to be constant throughout the heat wheel;
- heat wheel involves no work interactions so that kinetic and potential energy changes for each fluid are assumed to be negligible;
- the system is over-all adiabatic;
- fluids are assumed to be low velocity gases at essentially constant pressure so that enthalpy is treated as a function of temperature, using the specific heat property;
- the pressure along the entire heat wheel tube is assumed to be uniform.

Now, we are in a position to move to the development of the mathematical model for heat wheel dynamics.

2.2. Development of mathematical models

Based on the assumptions discussed in Section 2.1, differential equations relating the fluid and matrix temperatures can be derived from the energy balance equation applied to a unit element dz through the heat wheel for a control volume. In what follows, we denote by T the temperature of fluid and the matrix which is a function of time t and distance z, $T = T(t, z)$. Furthermore, in all discussions related to the fluid airflow we use subscript 'f' with f = (f_h, f_c) to indicate the air extracted from the room to the exhausted duct (denoted by f_h) or the air supplied from outdoor to the room (denoted by f_c). Note that for the laboratory-scale heat wheel considered in the present paper, the temperature of the extracted air is higher than that of the supply air. Hence, f_h is used to represent the hot air on the extracted fluid air side and f_c is used to represent the cold air on the supply fluid air side. Finally, we use subscript 'w' in our discussion of the wheel matrix.

Our starting point is the energy balance equation given in the following form [8]:

$$\dot{Q}_{\mathrm{in}} + \dot{W} + q''_{\mathrm{w-f}} = \dot{Q}_{\mathrm{out}} + \left(\frac{\mathrm{d}E}{\mathrm{d}t}\right)_{CV} \tag{2.1}$$

where $\dot{Q}_{\mathrm{in}} + \dot{W} + q''_{\mathrm{w-f}}$ is the energy-input rate with $\dot{Q}_{\mathrm{in}} = [\dot{m}\cdot(e+\mathrm{Pv})]_{\mathrm{in}} = [\dot{m}\cdot(\mathrm{KE}+\mathrm{PE}+u+\mathrm{Pv})]_{\mathrm{in}}$, e the total energy of the matter (fluid or gas) per unit mass, u the internal energy, KE the bulk kinetic energy, PE the bulk potential energy, Pv the flow work that is the amount of energy transfer as work (associated with a unit of mass), $\dot{W}$ the sum of shaft-power input and power input due to normal motion of the control-volume boundaries, $q''_{\mathrm{w-f}}$ the sum of all heat transfer rates from the wheel matrix to the fluid for the control volume, $\dot{Q}_{\mathrm{out}} = [\dot{m}\cdot(e+\mathrm{Pv})]_{\mathrm{out}}$ the energy-output rate and $\dot{E} = (\frac{\mathrm{d}E}{\mathrm{d}t})_{CV}$ is the energy-storage rate.

Our analysis is based on Eq. (2.1) considered in the one-dimensional approximation. Heat convection and heat conduction are analysed here in the fluid direction over the control volume of (a) each fluid airflow within cross-areas $A_{\mathrm{f_h}}$ and $A_{\mathrm{f_c}}$ and (b) the wheel matrix within cross-area A_{w}. Note that $A_{\mathrm{f_h}}$ and $A_{\mathrm{f_c}}$ are the sum of the areas of each channel on the fluid sides, while A_{w} is the effective area of the thin plate from the simplified wheel matrix. In Fig. 3, we present the diagram for model simplification and provide all necessary details of our definition of the control volume element definition.

We use Eq. (2.1) for control volume elements of the extracted air, the wheel matrix and the supply air. Fig. 4 illustrates our approach in greater details.

In particular, for the control volume elements presented in Fig. 4 we have the following relationships (written for the extracted air, the wheel matrix and the supply air, respectively):

$$\dot{Q}_{\mathrm{f_h},z+\mathrm{d}z} - \left(\lambda_{\mathrm{f_h}}\cdot A_{\mathrm{f_h}}\frac{\partial T_{\mathrm{f_h}}}{\partial z}\bigg|_{z+\mathrm{d}z} - \lambda_{\mathrm{f_h}}\cdot A_{\mathrm{f_h}}\frac{\partial T_{\mathrm{f_h}}}{\partial z}\bigg|_{z}\right) = \dot{Q}_{\mathrm{f_h},z} + q''_{\mathrm{f_h-w}} + \frac{\mathrm{d}E_{\mathrm{f_h}}}{\mathrm{d}t}, \tag{2.2}$$

$$\frac{\mathrm{d}E_{\mathrm{w}}}{\mathrm{d}t} = q''_{\mathrm{f_h-w}} - q''_{\mathrm{w-f_c}} + \left(\lambda_{\mathrm{w}}\cdot A_{\mathrm{w}}\frac{\partial T_{\mathrm{w}}}{\partial z}\bigg|_{z+\mathrm{d}z} - \lambda_{\mathrm{w}}\cdot A_{\mathrm{w}}\frac{\partial T_{\mathrm{w}}}{\partial z}\bigg|_{z}\right), \tag{2.3}$$

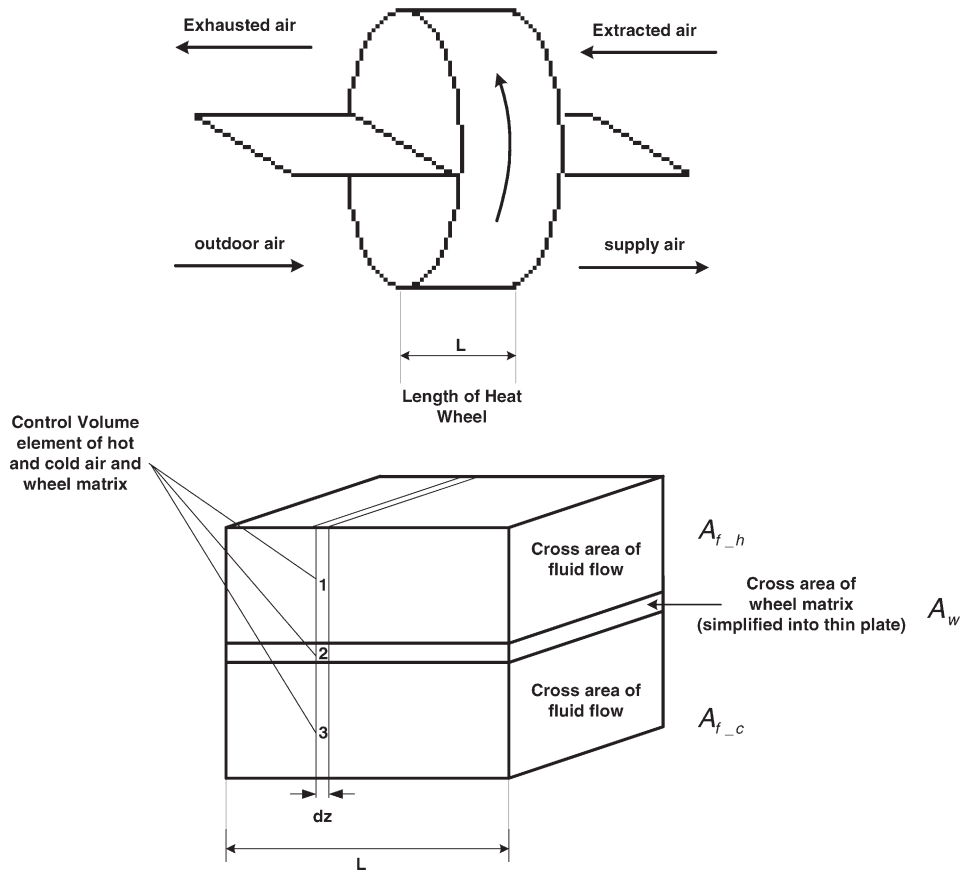

Fig. 3. Diagram of thermal model simplification and control volume element definition.

$$\dot{Q}_{\mathrm{f_c},z} + q''_{\mathrm{w-f_c}} + \left(\lambda_{\mathrm{f_c}} \cdot A_{\mathrm{f_c}} \frac{\partial T_{\mathrm{f_c}}}{\partial z}\bigg|_{z+\mathrm{d}z} - \lambda_{\mathrm{f_c}} \cdot A_{\mathrm{f_c}} \frac{\partial T_{\mathrm{f_c}}}{\partial z}\bigg|_{z}\right) = \dot{Q}_{\mathrm{f_c},z+\mathrm{d}z} + \frac{\mathrm{d}E_{\mathrm{f_c}}}{\mathrm{d}t}. \tag{2.4}$$

In (2.2)–(2.4), for both $\dot{Q}_{\mathrm{f_h}}$ and $\dot{Q}_{\mathrm{f_c}}$ we have (e.g., [9]):

$$\dot{Q} = \dot{m}h = \dot{m}c_{\mathrm{p}}\,\Delta T. \tag{2.5}$$

Furthermore, we have KE = 0, PE = 0 in $\dot{Q}$ and $u + \mathrm{Pv} = h$,

$$\frac{\mathrm{d}E}{\mathrm{d}t} = M\dot{h} = Mc_{\mathrm{p}}\,\frac{\mathrm{d}T}{\mathrm{d}t}, \tag{2.6}$$

$$q'' = U \cdot B_{\mathrm{w}}(T_{\mathrm{w}} - T_{\mathrm{f}})\,\mathrm{d}z \tag{2.7}$$

for both $E_{\mathrm{f_h}}$, $E_{\mathrm{f_c}}$, E_{w} and $q''_{\mathrm{f_h-w}}$, $q''_{\mathrm{w-f_c}}$. Finally, we mention that U is the overall heat transfer coefficient which will be dealt with in detail Section 2.3, and that

$$\lambda \cdot A\,\frac{\partial T}{\partial z}\bigg|_{z+\mathrm{d}z} - \lambda \cdot A\,\frac{\partial T}{\partial z}\bigg|_{z} = \left[\lambda \cdot A\,\frac{\partial T}{\partial z}\right]_{z}^{z+\mathrm{d}z} = \lambda \cdot A \int_{z}^{z+\mathrm{d}z} \frac{\partial}{\partial z}\left(\frac{\partial T}{\partial z}\right)\mathrm{d}\xi. \tag{2.8}$$

By substituting Eqs. (2.5)–(2.8) into Eqs. (2.2)–(2.4), we obtain a set of three equations:

- for the extracted air:

$$\dot{m}_{\mathrm{f_h}} h_{\mathrm{f_h},z+\mathrm{d}z} - \lambda_{\mathrm{f_h}} \cdot A_{\mathrm{f_h}} \int_{z}^{z+\mathrm{d}z} \frac{\partial}{\partial z}\left(\frac{\partial T_{\mathrm{f_h}}}{\partial z}\right)\mathrm{d}\xi = \dot{m}_{\mathrm{f_h}} h_{\mathrm{f_h},z} + \int_{z}^{z+\mathrm{d}z} B_{\mathrm{w}} U (T_{\mathrm{f_h}} - T_{\mathrm{w}})\,\mathrm{d}\xi + \frac{\partial}{\partial t}\int_{z}^{z+\mathrm{d}z} (A_{\mathrm{f_h}} \rho_{\mathrm{f_h}} h_{\mathrm{f_h}})\,\mathrm{d}\xi; \tag{2.9}$$

- for the supply air:

$$\dot{m}_{\mathrm{f_c}} h_{\mathrm{f_c},z} + \int_{z}^{z+\mathrm{d}z} B_{\mathrm{w}} U (T_{\mathrm{w}} - T_{\mathrm{f_c}})\,\mathrm{d}\xi + \lambda_{\mathrm{f_c}} \cdot A_{\mathrm{f_c}} \int_{z}^{z+\mathrm{d}z} \frac{\partial}{\partial z}\left(\frac{\partial T_{\mathrm{f_c}}}{\partial z}\right)\mathrm{d}\xi = \dot{m}_{\mathrm{f_c}} h_{\mathrm{f_c},z+\mathrm{d}z} + \frac{\partial}{\partial t}\int_{z}^{z+\mathrm{d}z} (A_{\mathrm{f_c}} \rho_{\mathrm{f_c}} h_{\mathrm{f_c}})\,\mathrm{d}\xi; \tag{2.10}$$

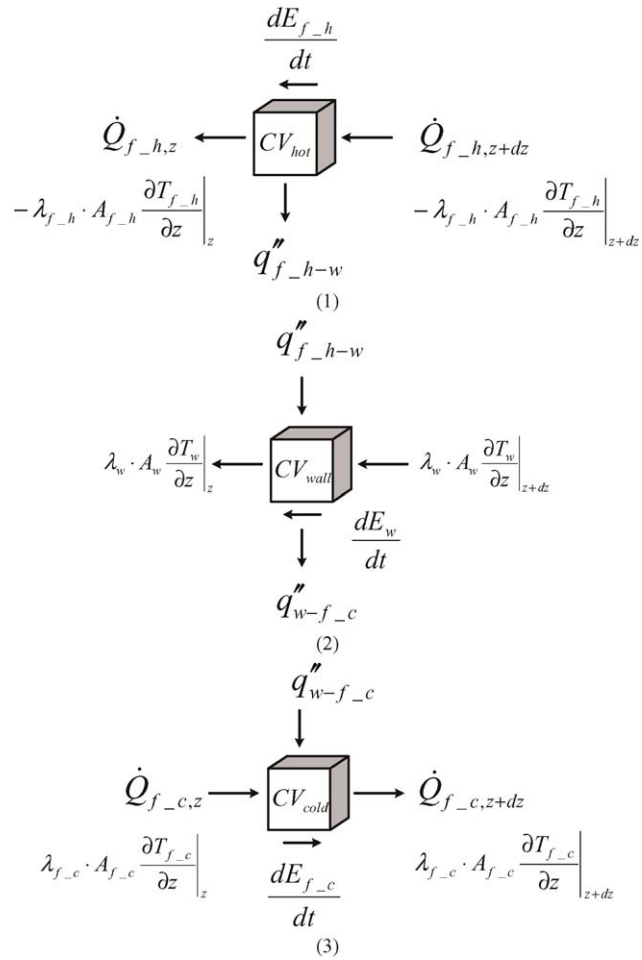

Fig. 4. Schematic diagram describing the energy balance analysis for a control volume of: (1) extracted air; (2) wheel matrix; (3) supply air.

- for the wheel matrix:

$$M_{\mathrm{w}} \cdot c_{\mathrm{p,w}} \cdot \frac{\partial T_{\mathrm{w}}}{\partial t} = UB_{\mathrm{w}}L(T_{\mathrm{f_h}} - T_{\mathrm{w}}) - UB_{\mathrm{w}}L(T_{\mathrm{w}} - T_{\mathrm{f_c}}) + \lambda_{\mathrm{w}} \cdot A_{\mathrm{w}} \cdot L\frac{\partial^2 T_{\mathrm{w}}}{\partial z^2}. \tag{2.11}$$

In the context of (2.9)–(2.11) we note that

$$\dot{m}_{\mathrm{f_h}} h_{\mathrm{f_h},z+\mathrm{d}z} - \dot{m}_{\mathrm{f_h}} h_{\mathrm{f_h},z} = [\dot{m}_{\mathrm{f_h}} h_{\mathrm{f_h}}]_z^{z+\mathrm{d}z} = \dot{m}_{\mathrm{f_h}} \int_z^{z+\mathrm{d}z} \frac{\partial h_{\mathrm{f_h}}}{\partial z}\,\mathrm{d}\xi, \tag{2.12}$$

$$\dot{m}_{\mathrm{f_c}} h_{\mathrm{f_c},z+\mathrm{d}z} - \dot{m}_{\mathrm{f_c}} h_{\mathrm{f_c},z} = [\dot{m}_{\mathrm{f_c}} h_{\mathrm{f_c}}]_z^{z+\mathrm{d}z} = \dot{m}_{\mathrm{f_c}} \int_z^{z+\mathrm{d}z} \frac{\partial h_{\mathrm{f_c}}}{\partial z}\,\mathrm{d}\xi, \tag{2.13}$$

$$h = c_{\mathrm{p}}(T - T_{\mathrm{ref}}) \tag{2.14}$$

for both $h_{\mathrm{f_h}}$ and $h_{\mathrm{f_c}}$, where h is enthalpy and c_{p} is specific heat.

We use (2.12)–(2.14) in (2.9) and (2.10) to get the model for the fluid part of the system:

- for the extracted air:

$$A_{\mathrm{f_h}}\rho_{\mathrm{f_h}} \int_z^{z+\mathrm{d}z} \frac{\partial h_{\mathrm{f_h}}}{\partial t}\,\mathrm{d}\xi = \dot{m}_{\mathrm{f_h}} \int_z^{z+\mathrm{d}z} \frac{\partial h_{\mathrm{f_h}}}{\partial z}\,\mathrm{d}\xi - B_{\mathrm{w}}U \int_z^{z+\mathrm{d}z} (T_{\mathrm{f_h}} - T_{\mathrm{w}})\,\mathrm{d}\xi - \lambda_{\mathrm{f_h}} \times A_{\mathrm{f_h}} \int_z^{z+\mathrm{d}z} \frac{\partial^2 T_{\mathrm{f_h}}}{\partial z^2}\,\mathrm{d}\xi \tag{2.15}$$

- for the supply air:

$$A_{\mathrm{f_c}}\rho_{\mathrm{f_c}} \int_z^{z+\mathrm{d}z} \frac{\partial h_{\mathrm{f_c}}}{\partial t}\,\mathrm{d}\xi = -\dot{m}_{\mathrm{f_c}} \int_z^{z+\mathrm{d}z} \frac{\partial h_{\mathrm{f_c}}}{\partial z}\,\mathrm{d}\xi + B_{\mathrm{w}}U \int_z^{z+\mathrm{d}z} (T_{\mathrm{w}} - T_{\mathrm{f_c}})\,\mathrm{d}\xi + \lambda_{\mathrm{f_c}} \times A_{\mathrm{f_c}} \int_z^{z+\mathrm{d}z} \frac{\partial^2 T_{\mathrm{f_c}}}{\partial z^2}\,\mathrm{d}\xi \tag{2.16}$$

Finally, taking into account that T_{ref} is a constant, which can be offset, final form of the mathematical model for the entire system can be written in the form of three coupled equations:

- for the extracted air:

$$\frac{\partial T_{\mathrm{f_h}}}{\partial t} = \frac{\dot{m}_{\mathrm{f_h}}}{A_{\mathrm{f_h}}\rho_{\mathrm{f_h}}} \frac{\partial T_{\mathrm{f_h}}}{\partial z} - \frac{B_{\mathrm{w}}U}{A_{\mathrm{f_h}}\rho_{\mathrm{f_h}}c_{\mathrm{p,f_h}}}(T_{\mathrm{f_h}} - T_{\mathrm{w}}) - \frac{\lambda_{\mathrm{f_h}}}{\rho_{\mathrm{f_h}}c_{\mathrm{p,f_h}}} \frac{\partial^2 T_{\mathrm{f_h}}}{\partial z^2}; \tag{2.17}$$

- for the supply air:

$$\frac{\partial T_{\mathrm{f_c}}}{\partial t} = -\frac{\dot{m}_{\mathrm{f_c}}}{A_{\mathrm{f_c}}\rho_{\mathrm{f_c}}} \frac{\partial T_{\mathrm{f_c}}}{\partial z} + \frac{B_{\mathrm{w}}U}{A_{\mathrm{f_c}}\rho_{\mathrm{f_c}}c_{\mathrm{p,f_c}}}(T_{\mathrm{w}} - T_{\mathrm{f_c}}) + \frac{\lambda_{\mathrm{f_c}}}{\rho_{\mathrm{f_c}}c_{\mathrm{p,f_c}}} \frac{\partial^2 T_{\mathrm{f_c}}}{\partial z^2}; \tag{2.18}$$

- for the wheel matrix:

$$\frac{\partial T_{\mathrm{w}}}{\partial t} = \frac{UB_{\mathrm{w}}L}{M \cdot c_{\mathrm{p,w}}}(T_{\mathrm{f_h}} - 2T_{\mathrm{w}} - T_{\mathrm{f_c}}) + \frac{\lambda_{\mathrm{w}}}{\rho_{\mathrm{w}} \cdot c_{\mathrm{p,w}}} \frac{\partial^2 T_{\mathrm{w}}}{\partial z^2}. \tag{2.19}$$

The resulting three coupled partial differential equations (PDEs) ((2.17)–(2.19)) written in terms of temperatures $T_{\mathrm{f_h}}$, $T_{\mathrm{f_c}}$ and T_{w} (as functions of z, t) should be supplemented by

appropriate initial and boundary conditions. In particular, we provide one initial and two boundary conditions at both ends for the air fluid. Further, we note that for the rotating wheel matrix (facing partially the hot and cold air sides during the process of transferring energy), the initial temperature of the wheel matrix facing the hot air side equal to the hot air initial temperature (when the rotational speed of the wheel is zero). Similarly, the initial temperature of the wheel matrix facing the cold air side is the same as the cold air initial temperature. For the sake of brevity, we use capital letter I for f_h, f_c and w in writing down the initial and boundary conditions of the problem:

$$T_I|_{t=0} = T_{I,0}, \quad \text{for } I = \text{f_h, f_c, w}, \tag{2.20}$$

where $T_w|_{t=0} = T_{f_h,0}$ on the hot air side and $T_w|_{t=0} = T_{f_c,0}$ on the cold air side,

$$\frac{\partial T_I}{\partial t}(t, z = 0) = 0, \quad \text{for } I = \text{f_h, w}, \tag{2.21}$$

$$\frac{\partial T_I}{\partial t}(t, z = L) = 0, \quad \text{for } I = \text{f_c, w}, \tag{2.22}$$

$$T_h(t, z = L) = T_{h,in}, \qquad T_c(T, z = 0) = T_{c,in}. \tag{2.23}$$

2.3. Evaluation of overall heat transfer coefficient

The model formulated in Section 2.2 requires an evaluation of the heat transfer coefficient. This coefficient characterises the overall heat transfer and includes both convective and conductive mechanisms responsible for the heat transfer from the hot fluid to the cold one. This can be expressed mathematically as follows (e.g., [10]):

$$\frac{d\dot{Q}}{dA} = U(T_{f_h} - T_{f_c}), \tag{2.24}$$

where $d\dot{Q}/dA$ is the heat flux per unit transfer area at a cross-section of the heat wheel, $(T_h - T_c)$ the difference between hot and cold air temperatures and U is the overall heat transfer coefficient.

A good approximation to U can be provided by the following simple representation: $U = 1/R_{total}$, where $R_{total} = R_w + R_f$ is the total heat transfer resistance which is a combination of the heat conduction resistance of the matrix and the heat convection resistance of the fluid (in particular, $R_f = 1/h_f$). In most practical problems, R_w is much smaller than R_f, so the value of forced convection coefficient h_f is the dominant term in the equation for U. Hence, the total heat transfer coefficient can be very well approximated as follows:

$$U = \frac{1}{\frac{1}{h_{f_h}} + \frac{1}{h_{f_c}}}, \tag{2.25}$$

where h_{f_h} and h_{f_c} represent the forced convective coefficient of the hot and cold air, respectively. The forced convective coefficient is governed by fluid dynamic phenomena, surface geometry, fluid properties and flow conditions. This coefficient can be correlated to Reynolds number $Re \equiv \bar{v}D_{hy}\rho/\mu$, Prandtl number $Pr \equiv \mu \cdot c_p/k$ and Nusselt number $Nu \equiv hL/k$. Recall that D_{hy}, is the hydraulic diameter and $\bar{v}$ is the velocity of the fluid (e.g., [11]), and in our notation $D_{hy} = D$, $\bar{v} = v$ while the other parameters are specified in 'Nomenclature'.

In the case considered in this paper, the parallel small diameter passages configured in the wheel matrix allow for high heat transfer rate at low pressure drop when air stream flow, in which case the aluminum spacers can be used for forming these passages to ensure the airflow is a laminar flow [12]. Therefore, we can use the Nusselt number for a laminar flow given as (e.g., [11]):

$$Nu = 3.66 + \frac{0.0668 \cdot (d/L) \cdot Re \cdot Pr}{1 + 0.04 \cdot [(d/L) \cdot Re \cdot Pr]^{2/3}} \tag{2.26}$$

This allows us to estimate the forced convection coefficients h_{f_h}, h_{f_c}, and hence, according to (2.25), the overall heat transfer coefficient.

2.4. Influence of the rotational speed of the wheel matrix

From experimental results performed for the laboratory-scale heat wheel, it is known that the dynamic behavior of heat wheel is dominated by several important parameters of the system. In particular, it is known that the influence of the rotational speed of the wheel ϕ (s^{-1}) upon the temperature and energy effectiveness can be substantial. Therefore, our next goal is to incorporate parameter ϕ into the mathematical model. Other factors, such as the airflow characteristics, ambient temperature and geometrical size of the wheel, will be discussed in Section 4.

Note that the heat exchange effectiveness for a rotary regenerator, denoted further by ε_{rotary}, can be characterised by parameter C_r/C_{min}, tailored to the rotary enthalpy of the wheel, where $C_r = M_w c_{p,w}\phi$ represents the thermal capacitance of the matrix [10,12]. In particular, we have

$$\varepsilon_{rotary} = \varepsilon_{\text{counter flow direct type}}\left[1 - \frac{1}{9\left[\frac{C_r}{C_{min}}\right]^{1.93}}\right] = \frac{\dot{Q}}{\dot{Q}_{max}} \tag{2.27}$$

where

$$\varepsilon_{\text{counter flow direct type}} = \frac{1 - e^{-\text{NTU}\cdot[1-(C_{min}/C_{max})]}}{1 - \frac{C_{min}}{C_{max}} e^{-\text{NTU}\cdot[1-(C_{min}/C_{max})]}} \tag{2.28}$$

is the heat exchange effectiveness of the counter-flow direct type heat exchanger, $\text{NTU} = \frac{UA_s}{C_{min}}$ the number of transfer unit [10], A_s the total surface which heat transferred through the matrix ($A_s = L \cdot B_w$), C_{min} and C_{max} the minimum and maximum heat capacitance values (found between C_{f_h} and C_{f_c}) and the term $[1 - \frac{1}{9[\frac{C_r}{C_{min}}]^{1.93}}]$ is a correction factor for the rotational speed

which accounts for how the matrix speed influences the heat recovery effectiveness. We note also that for the heat wheel, heat transfer is carried periodically, which means that the energy transferred varies with the frequency of wheel. Based on this observation, we multiply the energy source for control volume by the affecting factor $9[\frac{C_r}{C_{min}}]^{1.93}$ to arrive at the following generalisation of our model:

$$\frac{\partial T_{f_h}}{\partial t} = \frac{\dot{m}_{f_h}}{A_{f_h}\rho_{f_h}}\frac{\partial T_{f_h}}{\partial z} - 9\left[\frac{C_r}{C_{min}}\right]^{1.93} \times \frac{B_w U}{A_{f_h}\rho_{f_h}c_{p,f_h}}(T_{f_h} - T_w) - \frac{\lambda_{f_h}}{\rho_{f_h}c_{p,f_h}}\frac{\partial^2 T_{f_h}}{\partial z^2} \tag{2.29}$$

$$\frac{\partial T_{f_c}}{\partial t} = -\frac{\dot{m}_{f_c}}{A_{f_c}\rho_{f_c}}\frac{\partial T_{f_c}}{\partial z} + 9\left[\frac{C_r}{C_{min}}\right]^{1.93} \times \frac{B_w U}{A_{f_c}\rho_{f_c}c_{p,f_c}}(T_w - T_{f_c}) + \frac{\lambda_{f_c}}{\rho_{f_c}c_{p,f_c}}\frac{\partial^2 T_{f_c}}{\partial z^2} \tag{2.30}$$

$$\frac{\partial T_w}{\partial t} = 9\left[\frac{C_r}{C_{min}}\right]^{1.93} \cdot \frac{UB_w L}{M \cdot c_{p,w}}(T_{f_h} - 2T_w - T_{f_c}) + \frac{\lambda_w}{\rho_w \cdot c_{p,w}}\frac{\partial^2 T_w}{\partial z^2}. \tag{2.31}$$

Model (2.29)–(2.31) contains a number of fundamental parameters which are gathered for the convenience of the reader in 'Nomenclature' and Table A.1. These are parameters used in all our simulations discussed in detail in Sections 3 and 4. On the other hand, such parameters as viscosity, thermal conductivity and density (to name just a few) may vary considerably with temperature. However, such property-variation effects at a particular flow cross-section can be compensated for by evaluating certain or all of the properties at some specified reference temperature with respect to the bulk temperatures [11]. As an example, in Fig. 5, we present the flowchart of our computational iterative procedure for calculating the heat transfer coefficient according to the bulk temperature.

The input block presented in Fig. 5 includes the initial temperature, geometrical size and thermal properties of the fluids and the wheel matrix, as well as the volumetric airflow and the frequency of the wheel. The computation of the energy effectiveness is carried out according to Eq. (2.28), while the output temperatures $T_{f_h,out}$ and $T_{f_c,out}$ are calculated based on the following equation:

$$\varepsilon_{rotary} = \frac{\text{actual heat} - \text{transfer rate}}{\text{maximum possible heat} - \text{transfer rate}} = \frac{\dot{Q}}{\dot{Q}_{max}} \tag{2.32}$$

where the maximum possible heat transfer rate is $\dot{Q}_{max} = C_{min}(T_{f_h,in} - T_{f_c,in})$ and the heat recovered through the heat exchanger is $\dot{Q} = C_h(T_{f_h,in} - T_{f_h,out}) = C_c(T_{f_c,in} - T_{f_c,out})$. Further, $T_{f_h,in}$ is the extracted air temperature when $t = 0$, $T_{f_c,in}$ is the outdoor air temperature when $t = 0$, $T_{f_h,out}$ is the exhausted air temperature from the heat wheel to outside, $T_{f_c,out}$ is the supply air temperature from the heat wheel to the room in the final steady state. In this way, the output temperature from the heat wheel is determined theoretically and the obtained value can be used for comparisons with results of simulations.

3. Numerical methodology and results of simulation

In this section, we describe the process of simulation of the heat wheel based on an implicit algorithm resulted from a finited difference approximation. The developed procedure allows to simulate accurately both the steady-state behavior of the system as well as its dynamic response.

3.1. Numerical methodology

The mathematical model of the heat wheel (2.29)–(2.31) has been discretised with an implicit finite difference scheme constructed for all three coupled partial differential equations supplemented by boundary and initial conditions (2.20)–(2.23). The discretised equations have been solved by the Thomas algorithm. Below, we describe this discretisation procedure in detail. Firstly, we simplify our model as follows:

(A) Convection term (for the fluid):

$$E_f = \frac{\dot{m}_h c_{p,f}}{A_f \rho_f c_{p,f}} = \frac{\dot{v}_f}{A_f} = v_f \tag{3.1A}$$

with $\dot{m} = \dot{v} \cdot p = v \cdot \rho/A$.

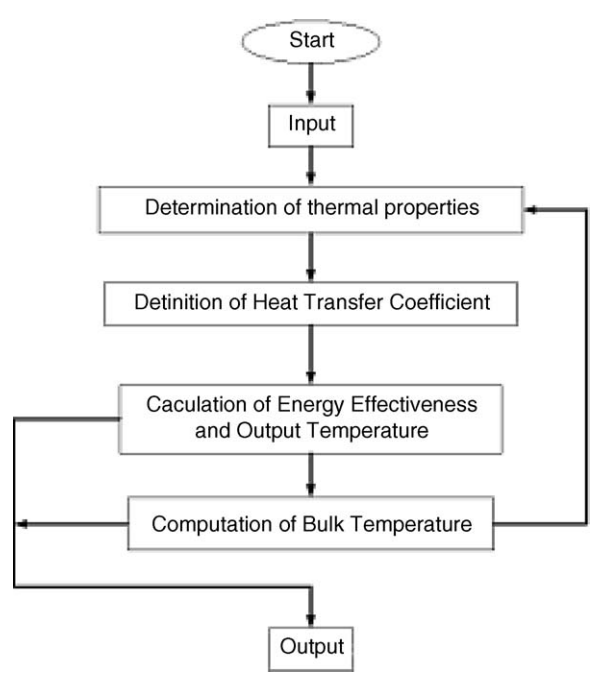

Fig. 5. Flowchart of parameter specification incorporated in the MATLAB computational program.

(B) Heat flux term (for the fluid and the wheel matrix):

$$F_{\mathrm{f}} = \frac{B_{\mathrm{w}} U}{A_{\mathrm{f}} \rho_{\mathrm{f}} c_{\mathrm{p,f}}}, \qquad F_{\mathrm{w}} = \frac{B_{\mathrm{w}} U L}{M \cdot c_{\mathrm{p,w}}}. \tag{3.1B}$$

(C) Conduction term (for the fluid and the wheel matrix):

$$G_{\mathrm{f}} = \frac{\lambda_{\mathrm{f}}}{\rho_{\mathrm{f}} \cdot c_{\mathrm{p,f}}}, \qquad G_{\mathrm{w}} = \frac{\lambda_{\mathrm{w}}}{\rho_{\mathrm{w}} \cdot c_{\mathrm{p,w}}}. \tag{3.1C}$$

Taking into account (3.1A)–(3.1C), we rewrite our model as follows:

$$\frac{\partial T_{\mathrm{f_h}}}{\partial t} = E_{\mathrm{f_h}} \frac{\partial T_{\mathrm{f_h}}}{\partial z} - F_{\mathrm{f_h}}(T_{\mathrm{f_h}} - T_{\mathrm{w}}) - G_{\mathrm{f_h}} \frac{\partial^2 T_{\mathrm{f_h}}}{\partial z^2}; \tag{3.2}$$

$$\frac{\partial T_{\mathrm{f_c}}}{\partial t} = -E_{\mathrm{f_c}} \frac{\partial T_{\mathrm{f_c}}}{\partial z} + F_{\mathrm{f_c}}(T_{\mathrm{w}} - T_{\mathrm{f_c}}) + G_{\mathrm{f_c}} \frac{\partial^2 T_{\mathrm{f_c}}}{\partial z^2}; \tag{3.3}$$

$$\frac{\partial T_{\mathrm{w}}}{\partial t} = F_{\mathrm{w}}(T_{\mathrm{f_h}} - 2T_{\mathrm{w}} - T_{\mathrm{f_c}}) + G_{\mathrm{w}} \frac{\partial^2 T_{\mathrm{w}}}{\partial z^2}. \tag{3.4}$$

Secondly, we use standard finite difference approximations $\frac{\partial T}{\partial t} = \frac{T_i^{j+1} - T_i^j}{\tau}$, $\frac{\partial^2 T}{\partial z^2} = \frac{T_{i+1}^{j+1} - 2T_i^{j+1} + T_{i-1}^{j+1}}{h^2}$ and $\frac{\partial T}{\partial t} = \frac{T_{i+1}^{j+1} - T_{i-1}^{j+1}}{2h}$, where $j = 1, 2, 3, \ldots, N_t$, $i = 1, 2, 3, 4, \ldots, N_z$, to arrive at the discretised equations for the air fluid and the wheel matrix:

for the extracted air:

$$A_{\mathrm{f_h}} T_{\mathrm{f_h}}^{j+1} - B_{\mathrm{f_h}} T_{\mathrm{w}}^{j+1} = T_{\mathrm{f_h}}^{j}; \tag{3.5}$$

for the supply air:

$$A_{\mathrm{f_c}} T_{\mathrm{f_c}}^{j+1} - B_{\mathrm{f_c}} T_{\mathrm{w}}^{j+1} = T_{\mathrm{f_c}}^{j}; \tag{3.6}$$

for the wheel matrix:

$$A_{\mathrm{w}} T_{\mathrm{w}}^{j+1} - B_{\mathrm{w}} T_{\mathrm{f_h}}^{j+1} - B_{\mathrm{w}} T_{\mathrm{f_c}}^{j+1} = T_{\mathrm{w}}^{j}. \tag{3.7}$$

In (3.5)–(3.7), $T_{\mathrm{f_h}}$, $T_{\mathrm{f_c}}$ and T_{w} are $N_z \times 1$ dimensional matrices, N_z is the number of the nodes in z direction of fluid flow which depend on the determination of the space step discretisation Δz (similarly, N_t is the number of computational iterations which depend on the definition of the time step discretisation τ), $A_I = \{a_{mn,I}\}$ and $B_I = \{b_{mn,I}\}$ are $N_z \times N_z$ dimensional matrices with m, $n = 1, 2, \ldots, N_z$, $I = \mathrm{f_h}, \mathrm{f_c}, \mathrm{w}$, where m is the row label and n is the column label. Both matrices A_I and B_I have the tridiagonal structure shown in Table 1.

Combining Eqs. (3.5)–(3.7), we obtain the following system of linear algebraic equations:

$$\begin{bmatrix} A_{\mathrm{f_h}} & 0 & -B_{\mathrm{f_h}} \\ 0 & A_{\mathrm{f_c}} & -B_{\mathrm{f_c}} \\ -B_{\mathrm{w}} & -B_{\mathrm{w}} & A_{\mathrm{w}} \end{bmatrix} \begin{bmatrix} T_{\mathrm{f_h}}^{j+1} \\ T_{\mathrm{f_c}}^{j+1} \\ T_{\mathrm{w}}^{j+1} \end{bmatrix} = \begin{bmatrix} T_{\mathrm{f_h}}^{j} \\ T_{\mathrm{f_c}}^{j} \\ T_{\mathrm{w}}^{j} \end{bmatrix}. \tag{3.8}$$

System (3.8) is solved in order to determine the steady-state temperature distribution for each point in the direction of fluid flow. The results of simulations are discussed next.

3.2. Results of simulations

The curves, shown in Fig. 6, provide the information on the temperature distributions for each fluid airflows as well as for the wheel matrix through the entire length heat wheel. The result demonstrates the steady state at each point in the fluid direction at the end of heating and cooling periods (iterations were performed until the error between two subsequent iterations did not exceed 10^{-5}). These results were compared with experimental results obtained for the laboratory-scale heat wheel. They showed an excellent agreement. Note that the temperature of the supply air from outdoor to the room increases from ambient temperature 275 K to around 293 K with the increase of the length of the heat wheel. At the same time, the temperature of the extracted air from the room to the exhausted duct decreases from 296 K to around 279 K. Finally, the wheel matrix temperatures are approximately equal to 278 and 294 K for $L = 0$ and 0.3, respectively, where L is the length of the heat wheel in meters. The results were obtained for the following values of the initial temperatures $T_{\mathrm{f_h}} = 296$ K, $T_{\mathrm{f_c}} = 275$ K, $T_{\mathrm{w}} = 275$ or 296 K with the discretisation time step of $\tau = 0.001$ s and $N_z = 20$.

Having succeeded in predicting average temperature distributions through the heat wheel for the fluids and the wheel matrix, we present also the dynamic responses of the

Table 1
Definition of matrix coefficients for discretised equations

m, n	$a_{mn,\mathrm{f_h}}$	$a_{mn,\mathrm{f_c}}$	$a_{mn,\mathrm{w}}$
$m = n = 2, 3, \ldots, N_z - 1$	$1 + \tau \cdot F_{\mathrm{f_h}} - \frac{2 \cdot \tau \cdot G_{\mathrm{f_h}}}{(\Delta z)^2}$	$1 + \tau \cdot F_{\mathrm{f_c}} - \frac{2 \cdot \tau \cdot G_{\mathrm{f_c}}}{(\Delta z)^2}$	$1 + 2\tau \cdot F_{\mathrm{w}} - \frac{2 \cdot \tau \cdot G_{\mathrm{w}}}{(\Delta z)^2}$
$m = n = 1$	$\frac{\tau \cdot E_{\mathrm{f_h}}}{2h} + 1 + \tau \cdot F_{\mathrm{f_h}} - \frac{\tau \cdot G_{\mathrm{f_h}}}{h^2}$	1	$1 + 2\tau \cdot F_{\mathrm{w}} - \frac{\tau \cdot G_{\mathrm{w}}}{h^2}$
$m = n = N_z$	1	$\frac{\tau \cdot E_{\mathrm{f_c}}}{2h} + 1 + \tau \cdot F_{\mathrm{f_c}} - \frac{\tau \cdot G_{\mathrm{f_c}}}{h^2}$	$1 + 2\tau \cdot F_{\mathrm{w}} - \frac{\tau \cdot G_{\mathrm{w}}}{h^2}$
$m - n = 1$	$\frac{\tau \cdot E_{\mathrm{f_h}}}{2h} + \frac{\tau \cdot G_{\mathrm{f_h}}}{h^2}$	$-\frac{\tau \cdot E_{\mathrm{f_c}}}{2h} - \frac{\tau \cdot G_{\mathrm{f_c}}}{h^2}$	$-\frac{\tau \cdot G_{\mathrm{w}}}{h^2}$
$n - m = 1$	$\frac{\tau \cdot G_{\mathrm{f_h}}}{h^2} - \frac{\tau \cdot E_{\mathrm{f_h}}}{h}$	$\frac{\tau \cdot E_{\mathrm{f_c}}}{2h} - \frac{\tau \cdot G_{\mathrm{f_c}}}{h^2}$	$-\frac{\tau \cdot G_{\mathrm{w}}}{h^2}$
	$b_{mn,\mathrm{f_h}}$	$b_{mn,\mathrm{f_c}}$	$b_{mn,\mathrm{w}}$
$m = n = 1, 2, \ldots, N_z - 1$	$\tau \cdot F_{\mathrm{f_h}}$		
$m = n = 2, \ldots, N_z$		$\tau \cdot F_{\mathrm{f_c}}$	
$m = n = 1, 2, \ldots, N_z$			$\tau \cdot F_{\mathrm{w}}$

Other elements not defined in this table are zero.

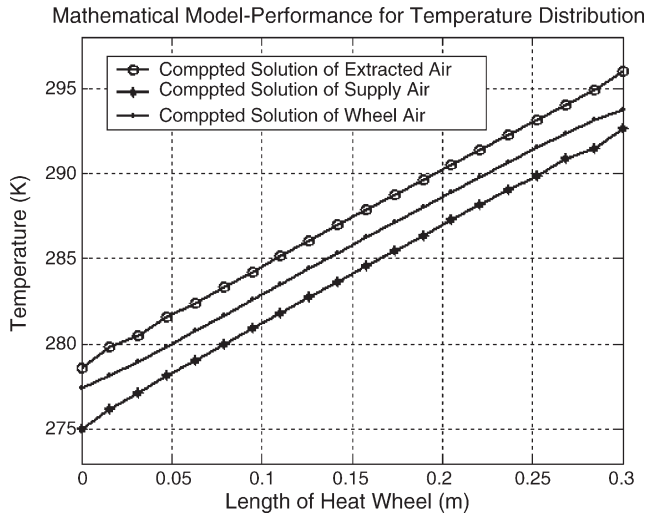

Fig. 6. Steady-state temperature distributions of fluid flows and wheel matrix through the heat wheel.

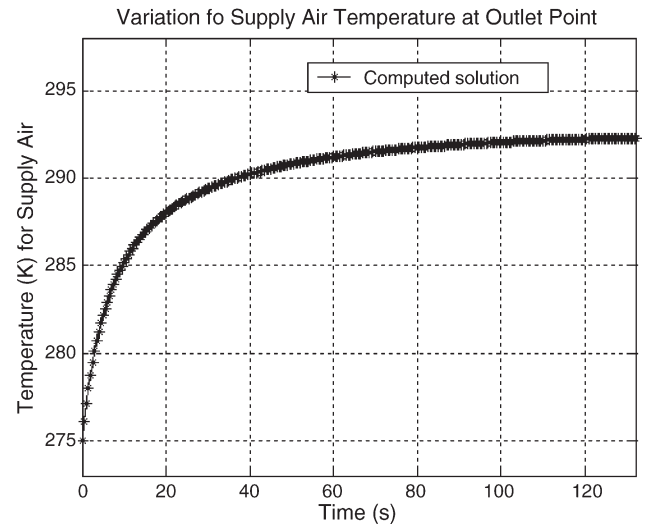

Fig. 8. Dynamic response of temperature variations of the outlet point of the extracted air when T_{f_h} = 296 K, T_{f_c} = 275 K and T_w = 296 K.

system in terms of temperature variations of the two fluids at the outlet point (see Figs. 7 and 8).

By analysing curves presented in Figs. 7 and 8, we conclude that the reacting effectiveness of the system is around 100 s. This means that when the rotating speed of the heat wheel is 6 rpm and the airflow on both sides is 0.25 m^3/s (while the other parameters are specified in Table A.2), the output temperature from the heat wheel needs 100 s to increase/decrease until it arrives at the steady state. The time constant should be mainly attributed to the energy storage in the wheel matrix and the heat conduction in it (characterised quantitatively by the second derivative of the T_w with respect to z).

The above results have been confirmed by solving the problem with the finite element methodology, implemented in a MATLAB-based package FEMLAB.

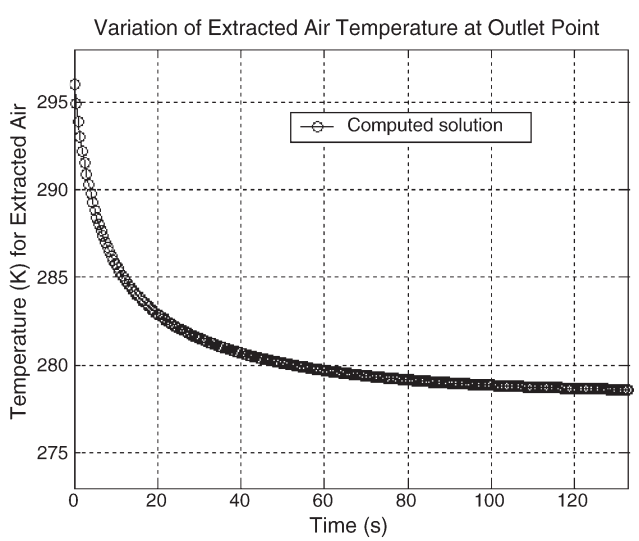

Fig. 7. Dynamic response of temperature variations at the outlet point of the supply air when T_{f_h} = 296 K, T_{f_c} = 275 K and T_w = 275 K.

4. Theoretical verification and experimental comparisons

In this section, we compare the results of numerical simulations obtained with the developed mathematical model for the heat wheel with those available from theoretical predications (in particular, for the energy effectiveness), as well as with experimental results obtained in the analysis of the dynamic behavior of the heat wheel.

4.1. Analysis of the factors of major influence

In what follows, we focus our attention on dominant factors that affect the performance of the developed model. As we discussed before, the rotational speed of the wheel is one of the important parameters that may have a substantial effect on the energy effectiveness by changing the output temperature directly. It is also important to note that the dynamic responses may be dependent in a non-trivial manner on variations of the input temperature and airflow. Furthermore, different geometries of the heat wheel are likely to influence the overall performance of the model in different ways. The effect of different geometries can be simulated by reducing the actual geometry of the wheel to a tube-like geometry and considering variations in the effective length, diameter and surface area of the wheel.

Our analysis here is based on three test cases for variable (a) frequency, (b) volumetric airflow and (c) input temperature, with fixed geometries. Other parameters are all assumed to be constants. It should be noted that further analysis is required for some such parameters (e.g., experiments show that the airflow input to the heat wheel model can behave like a ramp function).

The results of our analysis are shown in Fig. 9, while the corresponding input parameters are summarised in Table 2. The results presented demonstrate the influence of the

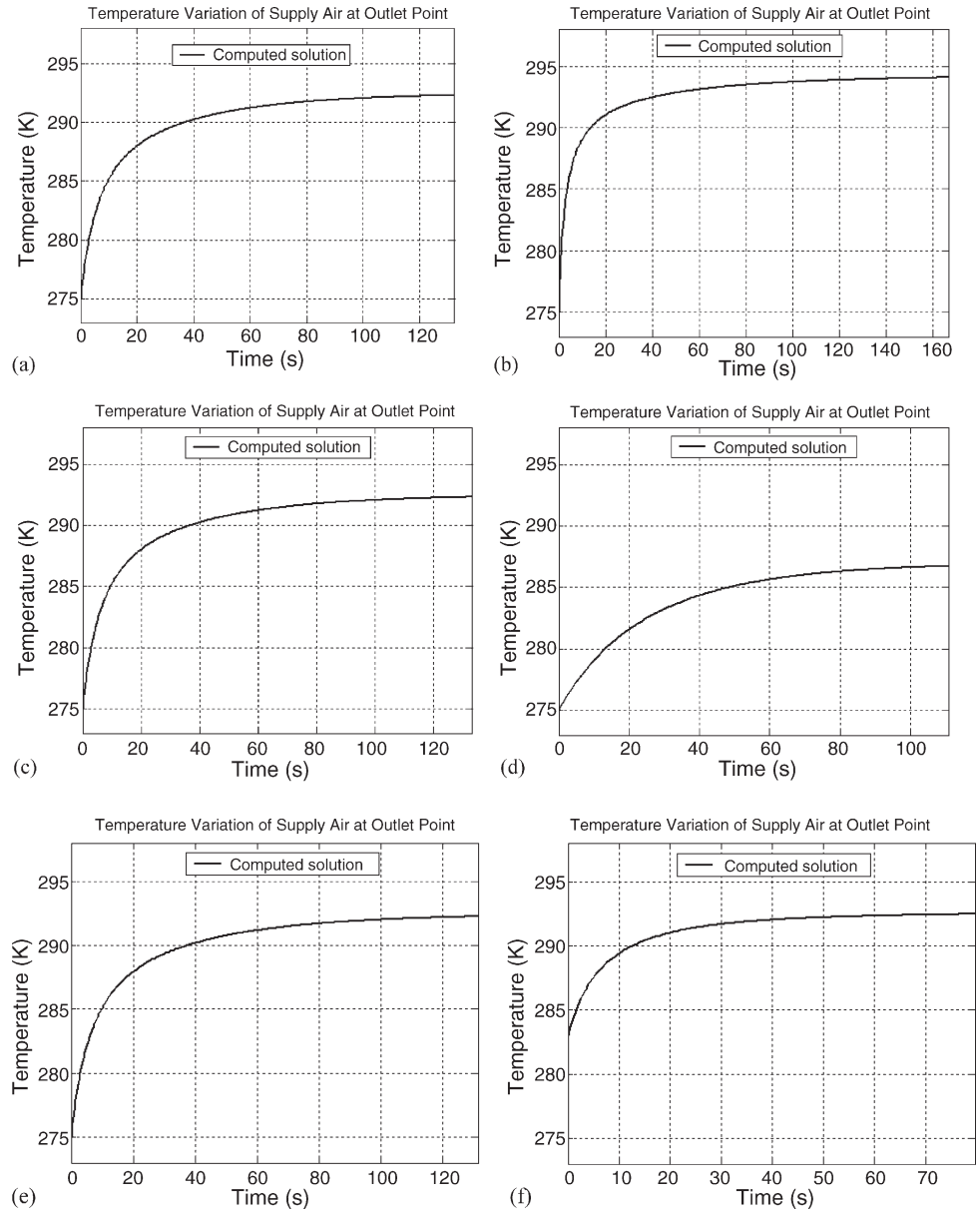

Fig. 9. Dynamic responses of the heat wheel model: (a) case 1, $\phi = 6$ Hz; (b) case 1, $\phi = 9$ Hz; (c) case 2, $\dot{v}_{f_h} = 0.35\,m^3/s$, $\dot{v}_{f_c} = 0.25\,m^3/s$; (d) case 2, $\dot{v}_{f_h} = 0.15\,m^3/s$, $\dot{v}_{f_c} = 0.30\,m^3/s$; (e) case 3, $T_{f_h,in}$ decreases from 296 to 293 K; (f) case 3, $T_{f_c,in}$ increases from 275 to 283 K.

parameters on the dynamic responses of the heat wheel model. In each of the three cases analysed here the results are presented for two different parameters. The time step τ for all simulation results reported here was chosen 0.001 s.

Case 1. Variable frequency of wheel matrix: $\phi = 6$ and 8 Hz.
Constant: $\dot{v}_{f_h} = 0.25\,m^3/s$, $\dot{v}_{f_c} = 0.25\,m^3/s$, $T_{f_h,in} = 296$ K, $T_{f_c,in} = 275$ K.

Case 2. Variable volumetric airflow: $\dot{v}_{f_h} = 0.35\,m^3/s$, $\dot{v}_{f_c} = 0.25\,m^3/s$; $\dot{v}_{f_h} = 0.15\,m^3/s$, $\dot{v}_{f_c} = 0.30\,m^3/s$.
Constant: $\phi = 6$ Hz, $T_{f_h,in} = 296$ K, $T_{f_c,in} = 275$ K.

Case 3. Variable input temperature: $T_{f_h,in} = 293$ K, $T_{f_c,in} = 275$ K; $T_{f_h,in} = 296$ K, $T_{f_c,in} = 283$ K.
Constant: $\dot{v}_{f_h} = 0.25\,m^3/s$, $\dot{v}_{f_c} = 0.25\,m^3/s$, $\phi = 6$ Hz.

The results of the analysis of variable inputs used in the model lead to quantification of the following conclusions drawn from Fig. 9. Firstly, from the results presented in Fig. 9(a and b) we conclude that the frequency of the wheel has an effect on the output temperature, and the faster the rotating speed, the higher the temperature of the heat wheel. Next, we note that by applying different ratios of hot to cold airflows, the output temperature will reach higher values with larger ratios

Table 2
Simulation parameters and specifications for the three cases analysed in Section 4.1

Parameters	Values
$T_{f_h,in}$	Variable
$T_{f_c,in}$	Variable
T_w	Variable
$\dot{v}_{f_h}$	Variable
$\dot{v}_{f_c}$	Variable
d	0.003
D	0.3
M	20
L	0.3
B_w	2.5
$c_{p,w}$	896
k_w	204
ρ_w	2707
ϕ	Variable

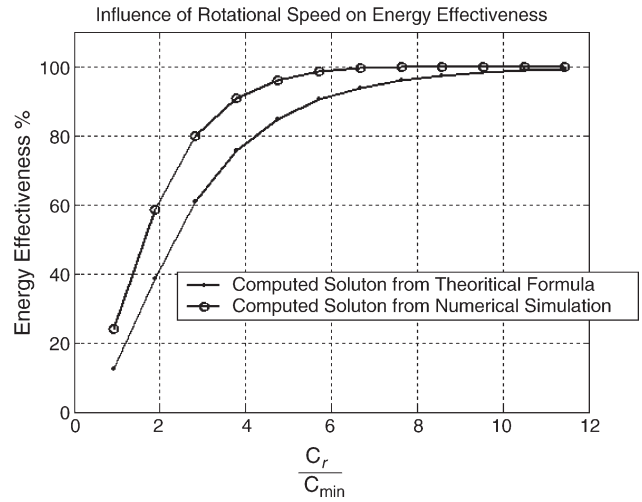

Fig. 11. Comparison of theoretical and simulation results obtained for different values of the ratio of heat capacitance.

compared top those with small ratios, as demonstrated by Fig. 9(c and d). As a consequence, we note further that by increasing the extracted airflow and decreasing the supply airflow, the temperature effectiveness of the system can be raised. Finally, we note that, as follows from Fig. 9(e and f), the starting point and the steady-state value will change accordingly to the input temperature of the extracted and supply air.

4.2. Theoretical verification

In this section we compare the results of our simulations with theoretical predictions for the energy efficiency. In particular, to obtain such predications we use Eq. (2.32) for different rotating speeds of the wheel. In Figs. 10 and 11, we show the variation in energy effectiveness with respect to C_r/C_{min}, where $C_r = M \cdot c_{p,w} \cdot \phi$. The geometries considered here are specified in Table A.1 and we use the same computational procedure, as the one presented in Fig. 5, to determine thermal properties of the system. Two main cases have been given major attention.

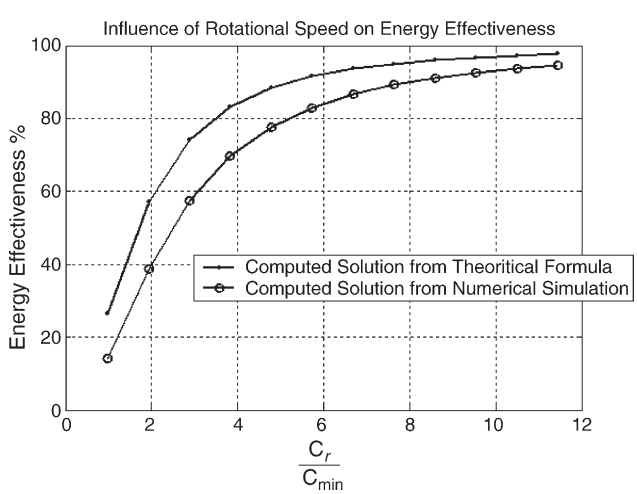

Fig. 10. Comparison of the energy efficiency: data obtained from numerical simulations and data obtained theoretical predictions.

Case 1. The primary controllable input settings are: $C_{min}/C_{max} = 0.9818$, $v_{f_h} = 0.25\,m^3/s$, $v_{f_c} = 0.25\,m^3/s$, $T_{f_c,in} = 2\,°C$, $T_{f_h,in} = 23\,°C$, $\phi = 6$ rpm.

Case 2. The primary controllable input settings are: $C_{min}/C_{max} = 0.7252$, $v_{f_h} = 0.35\,m^3/s$, $v_{f_c} = 0.25\,m^3/s$, $T_{f_c,in} = 2\,°C$, $T_{f_h,in} = 23\,°C$, $\phi = 6$ rpm.

Given the simplifying assumptions and estimations we use in the model, two curves presented in Figs. 10 and 11 are in reasonable agreement and the main trend of the energy efficiency curve is very well captured by our numerical experiments. Firstly, we note that the energy effectiveness is higher for cases having small C_{min}/C_{max} values with large hot airflows. Secondly, the effectiveness increases sharply with the increase of the rotational speed for small values of C_r/C_{min}. However, the rate of increase becomes slower after $C_r/C_{min} \cong 6$. This trend is in agreement with the results obtained from experiments.

4.3. Discussion of experimental results

Finally, we report results of our experiments with the actual ventilation unit with heat wheel. We have analysed the system response based on changes in main control inputs, which are specified in Table 3. In Fig. 12(a and b), we present the data obtained from the system operating at selected specific operating conditions (that is Case Nos. 1 and 2 specified in Table 3).

The differences between numerical simulations and experimental results are attributed to the fact that our experimental

Table 3
The main controllable input settings

	Parameters				
	$\dot{v}_{f_h}$ (m^3/s)	$\dot{v}_{f_c}$ (m^3/s)	ϕ (Hz)	$T_{f_c,in}$ (°C)	$T_{f_h,in}$ (°C)
Case No. 1 (a)	0.25	0.25	1	19.4	23.2
Case No. 2 (b)	0.25	0.25	5	20.3	23.3

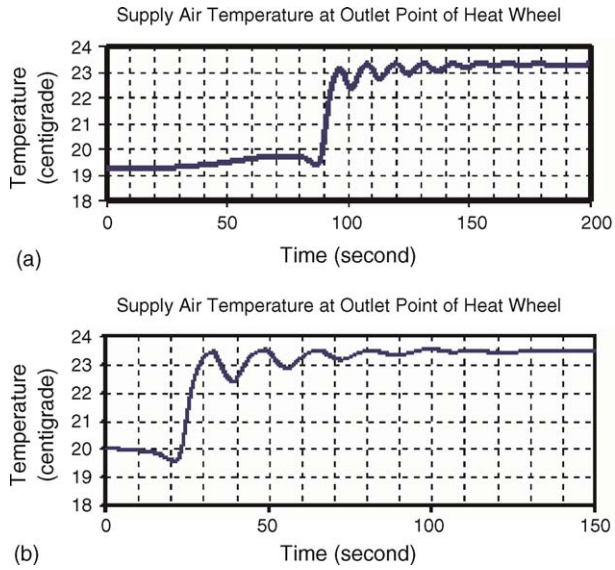

Fig. 12. (a and b) The supply air temperature variations at outlet point of heat wheel obtained from experimental measurement.

setups did not allow us to use the same input temperature and rotational speed as those considered in the numerical simulations. Furthermore, a multitude of parameters in the actual system are not constants as it was assumed in our model and they vary with variations in temperature. Finally, we note that the model was constructed with simplifying assumptions, e.g., without considering the heat dissipation of the wheel matrix. Given these limitations, in both cases presented in Table 3 numerical simulations and experimental results are in reasonable agreement in terms of temperature trends and steady-state values.

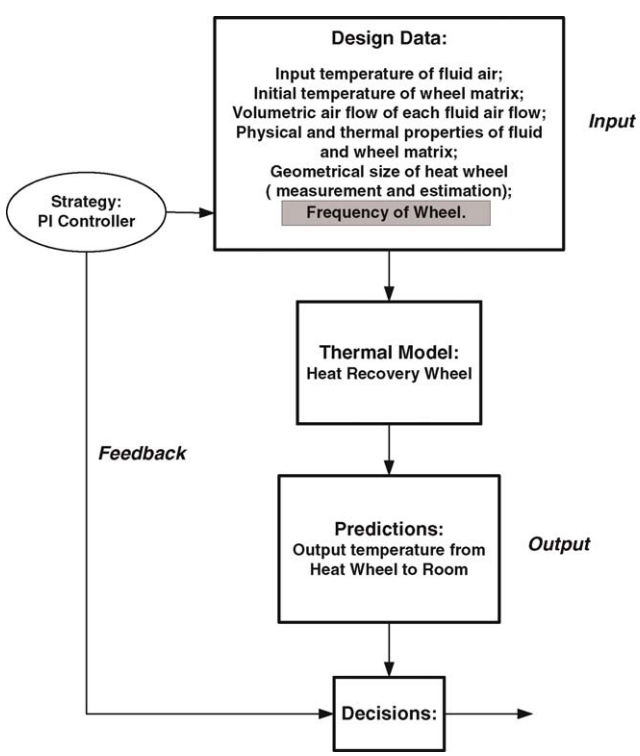

Fig. 13. Concept of temperature regulation system design.

The heat recovery system is a complex thermo-fluid device, and significant savings in energy can be achieved in such a system based on efficient control strategies. Fig. 13 illustrates the concept of temperature regulation system with a conventional PI controller based on the mathematical model of the heat wheel developed in this paper. It is one of the most important control systems in the entire ventilation unit which, from a control-theoretic point of view, is a complex multi-input–multi-output (MIMO) system.

5. Conclusions

We have developed a model of the regenerative heat wheel, a major component of ventilation units. For the developed model, we have proposed an efficient algorithm for its numerical

Table A.1
Parameter specifications of a laboratory-scale heat recovery wheel at the specified conditions

A_f (m^2)	0.0707
D (m)	0.3
d (m)	0.003
L (m)	0.3
B_w (m)	2.5
$T_{h,in}$ (°C)	23
$T_{c,in}$ (°C)	2
$\dot{v}_h$ (m^3/s)	0.25
$\dot{v}_c$ (m^3/s)	0.25
$c_{p,w}$ (J/(kg °C))	896
ϕ (Hz (s^{-1}))	6 (0–12)
M (kg)	20
ρ_h (kg/m^3)	1.2405
ρ_c (kg/m^3)	1.2542
$c_{p,h}$ (kJ/(kg °C))	1005.6
$c_{p,c}$ (kJ/(kg °C))	1005.6
μ_h (kg/(m s))	1.7800e−005
μ_c (kg/(m s))	1.7655e−005
k_h (W/(m °C))	0.0252
k_c (W/(m °C))	0.0249
$\dot{m}_h$ (kg/s)	0.3101
$\dot{m}_c$ (kg/s)	0.3136
v_h (m/s)	3.5368
v_c (m/s)	3.5368
h_h (W/(m^2 °C))	33.3446
h_c (W/(m^2 °C))	33.0860
R (m^2 °C/W)	0.0602
C_h (J/(s °C))	311.8472
C_c (J/(s °C))	315.3088
U (W/(m^2 °C))	94.5
$T_{h,out}$ (°C)	4.9680
$T_{c,out}$ (°C)	19.8340
Re_h	739.4202
Re_c	753.7820
Pr_h	0.7110
Pr_c	0.7117
Nu_h	3.9733
Nu_c	3.9792
C_r	1792
Ratio	0.9890
NTU	5.8815
ε_{cf}	0.8587

Table A.2
Properties of air at atmospheric pressure [11]

T (K)	ρ (kg/m)	c_p (kJ/(kg °C))	$\mu \times 10^5$ (kg/m s)	$v \times 10^6$ (m^2/s)	k (W/(m °C))	$\alpha \times 10^4$ (m^2/s)	Pr
250	1.4128	1.0053	1.5990	11.31	0.02227	0.15675	0.722
300	1.1774	1.0057	1.8462	15.69	0.02624	0.22160	0.708

implementation. We implemented the algorithm within MATLAB programming environment and presented the results of numerical simulations for the steady-state temperature distributions of fluid airflows and the wheel matrix through the entire length of the heat wheel. We have also analysed the influence of variations in rotating speed of the wheel as well as other characteristics on dynamic responses. The numerical results have been compared with experimental measurements and with theoretical predications of energy efficiencies.

Appendix A

See Tables A.1 and A.2.

References

[1] S.B. Riffat, M.C. Gillott, Performance of a novel mechanical ventilation heat recovery heat pump system, Applied Thermal Engineering 22 (2002) 839–845.
[2] F. Steimle, J. Roben, Ventilation requirements in modern buildings, in: Proceedings of the 13th AIVC conference, Nice, France, 1992, pp. 414–422.
[3] M.W. Liddament, A Guide to Energy Efficient Ventilation, Air Infiltration and Ventilation Center, 1996.
[4] N. Ghodsipour, M. Sddrdmeli, Experimental and sensitivity analysis of a rotary air preheater for the flue gas heat recovery, Applied Thermal Engineering 23 (2003) 571–580.
[5] R.K. Shah, T. Skiepko, Influence of leakage distribution on the thermal performance of a rotary regenerator, Applied Thermal Engineering 19 (1999) 685–705.
[6] O. Buyukalaca, T. Yilmaz, Influence of rotational speed on effectiveness of rotarytype heat exchanger, Heat and Mass Transfer 38 (2002) 441–447.
[7] A.L. London, F.R. Biancardi, J.W. Mitchell, The transient response of gas-turbine–plant heat exchangers–regenerators, intercoolers, precoolers, and ducting, Engineering for Power 81 (1959) 433–448.
[8] W.C. Reynolds, H.C. Perkins, Engineering Thermodynamics, second ed., McGraw-Hill, Inc., 1970.
[9] Y.A. Cengel, M.A. Boles, Thermodynamics: An Engineering Approach, third ed., McGraw-Hill, 1998.
[10] W.M. Kays, A.L. London, Compact Heat Exchangers, third ed., Krieger Publishing Company, 1984.
[11] F. Kreith, M.S. Bohn, Principles of Heat Transfer, fifth ed., PWS Publishing Company, 1997.
[12] S.J. Slayzak, J.P. Ryan, Desiccant Dehumidification Wheel Test Guide, National Renewable Energy Laboratory, 2000.